Figure 2: Records of CO_2 emissions, CO_2 concentrations, and Northern Hemisphere average surface temperature for the past 1000 years: (a) Reconstruction of past emissions of CO_2 as a result of land clearing and fossil fuel combustion since about 1750 (in billions of metric tons of carbon per year) [data from CDIAC, 2000; Andres et al., 2000; Marland et al., 1999; Houghton, 1995; Houghton and Hackler, 1995]; (b) Record of the CO_2 concentration for the last 1000 years, derived from measurements of CO_2 concentration in air bubbles in the layered ice cores drilled in Antarctica, a location that has been found to be representative of the global average concentration [data from Etheridge et al., 1998; Keeling and Whorf, 1999]; (c) Reconstruction of annual-average Northern Hemisphere surface air temperatures based on paleoclimatic records (Mann et al., 1999). For the Mann et al. data, the zero change baseline is based on the average conditions over the period 1902-80. The error bars for the estimate of the annual-average anomaly increase somewhat going back in time, with one standard deviation being about 0.25˚F (0.15˚C). Although this record comes mostly from the Northern Hemisphere, it is likely to be a good approximation to the global anomaly based on comparisons of recent patterns of temperature fluctuations.

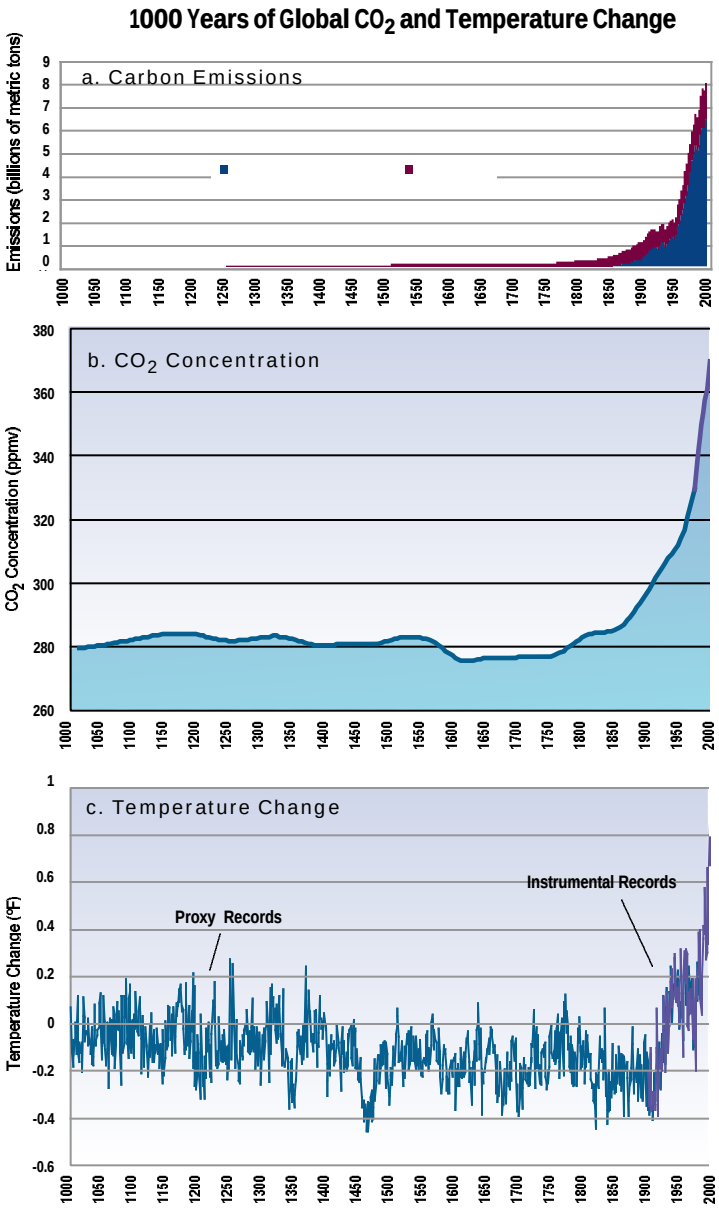

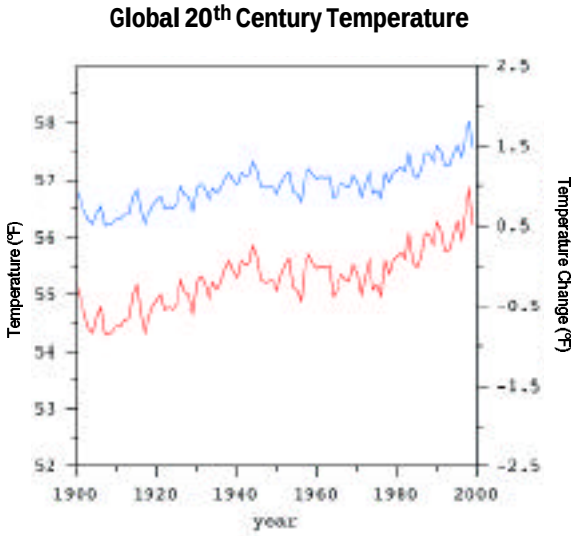

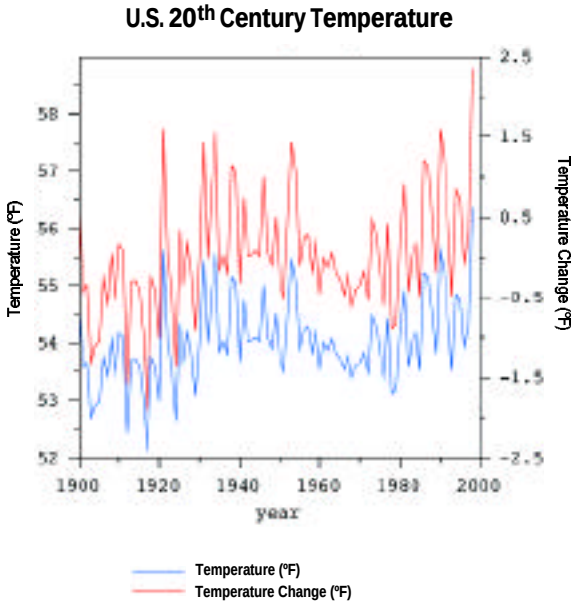

Figure 3: (a) Global annual-average surface temperature and temperature change for combined land and ocean regions for the period 1900-1999 based on the method of Quayle et al. (1999); (b) US annual-average surface temperature and temperature change for the period 1900-1999 using the USHCN data set (Easterling et al., 1996).

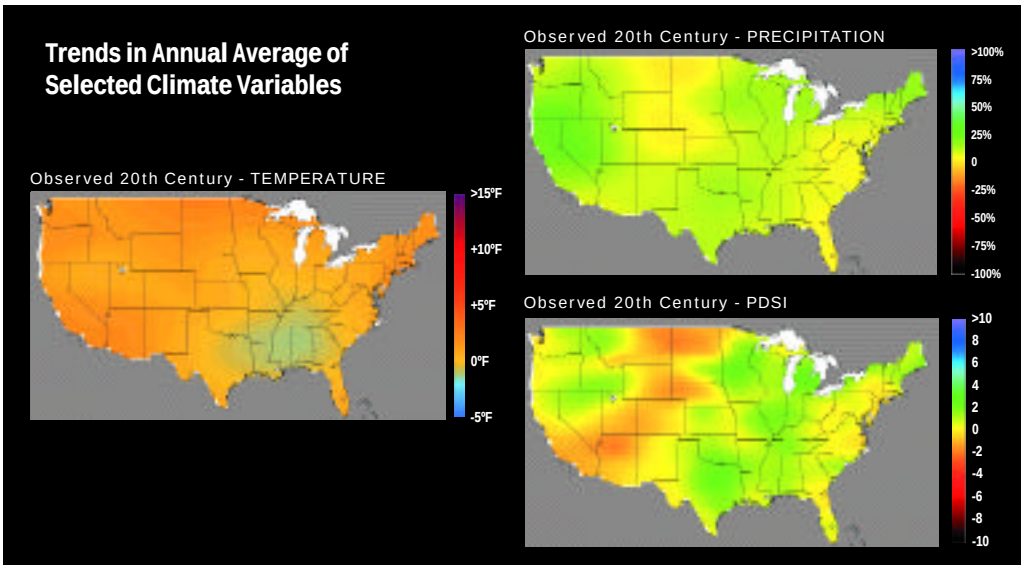

Figure 4: Trends in the annual average of selected climatic variables over the US during the 20th century as derived from observations compiled in the USHCN data set (Easterling et al., 1996). (a) Temperature (°F/century); (b) Precipitation (percent change/century); (c) Palmer Drought Severity Index (percent change/century).

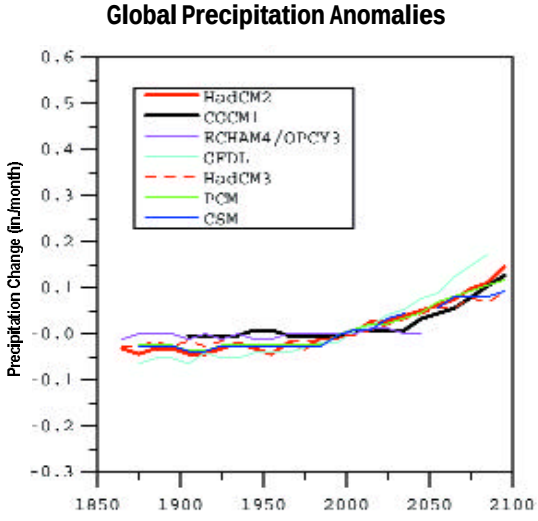

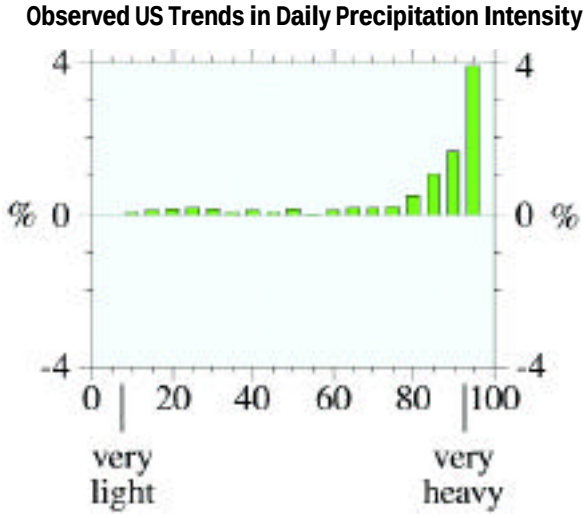

Figure 5: US trends (1910-1996) in mean precipitation (in percent change per century) for various categories of daily precipitation intensity. Values are plotted for each 5%, such that 5 represents from the lowest to 5th percentile and 95 represents the 95th to highest values of precipitation intensity. The lowest to 5th percentile are the lightest daily precipitation amounts and the 95th to highest are the heaviest daily amounts (Karl and Knight, 1998).

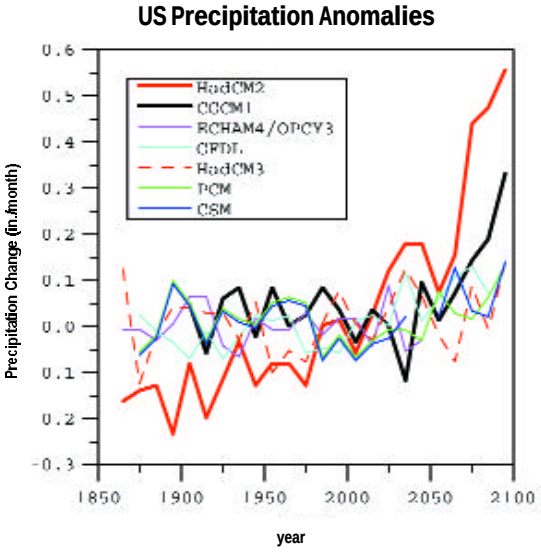

Figure 8: Comparison of the annual average changes in (a) global average precipitation (inches per month), and (b) average precipitation over the US from the Canadian model scenario and Hadley model scenario simulations used in the National Assessment and from the simulations of other groups (same as for Figure 7). The baseline period is assumed to be 1961-1990. Although decadal means have been applied to suppress year-to-year fluctuations, the greater variability of precipitation than temperature still reveals significant variations due to natural factors; the magnitude, although not the timing, of the remaining fluctuations may be considered plausible. The anomalies are with respect to the year 2000, calculating the values from a 2nd order polynomial fit.

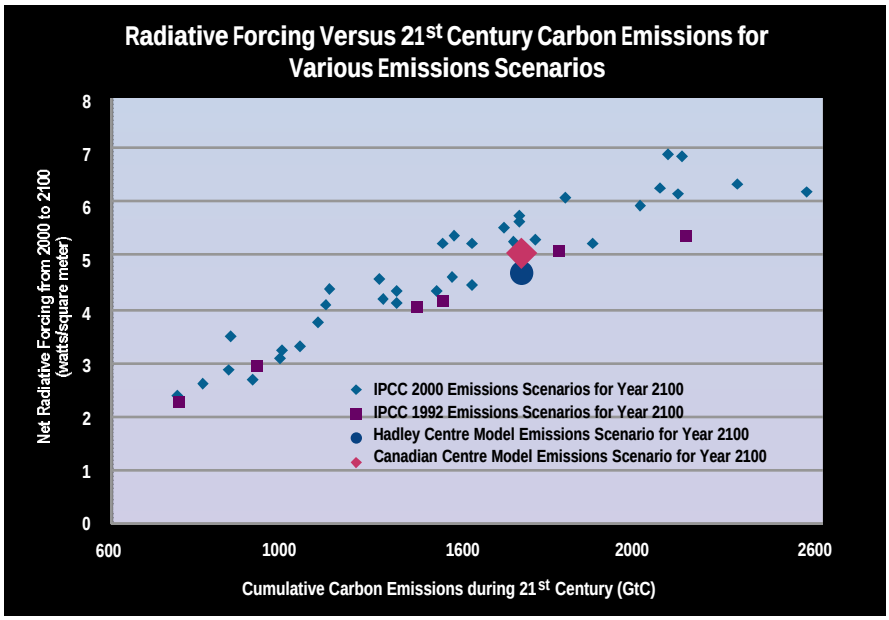

Figure 6: Comparison of the projections of total carbon emissions and overall human-induced radiative forcing for the six emissions scenarios prepared by the IPCC in 1992 (IS92 scenarios; IPCC, 1992) and the 35 emissions scenarios prepared by the IPCC in 2000 for which radiative forcing could be estimated (SRES scenarios; IPCC, 2000). These scenarios are based, although in different ways, on projected changes in emissions resulting from changes in population, economic development, energy use, efficiency of energy use, the mix of energy technologies, etc. The horizontal axis gives the total emissions of fossil fuel-derived carbon dioxide projected for the 21st century (in billions of tonnes of carbon, GtC). For reference, if the current level of global carbon emissions is maintained from 2000 to 2100, cumulative emissions over the 21st century would be roughly 650 GtC. Assuming no climate-related controls on emissions are introduced, this value is near the lowest value projected by any of the scenarios for the 21st century. The vertical axis gives the projected change in net radiative forcing at a pressure level approximating the tropopause (in watts per square meter) for all human-induced changes in greenhouse gases and aerosols (both direct and indirect contributions) over the 21st century using relationships employed in the IPCC Second Assessment Report (IPCC, 1996a; Smith et al., 2000), including the uptake of CO_2 by the oceans and land. Radiative forcing is important because it is the driving force for global warming; for reference, the projected change in radiative forcing up to the year 1992 is about 1.6 watts per square meter (IPCC, 1996a). The figure also shows the net radiative forcing and the approximate emissions of carbon used in the Hadley and Canadian scenarios. For these scenarios, which increase the equivalent CO_2 concentration by 1% per year, the carbon emissions are estimated by calculating the emissions needed to match the net radiative forcing after subtracting the radiative effects of other greenhouse gases and aerosols based on the average of IS92a and IS92f scenarios, and is an amount between the IS92a and IS92f scenarios. Based on these calculations, the Canadian and Hadley scenarios lie near the mid-range of the proposed scenarios in terms of both carbon emissions and net radiative forcing.

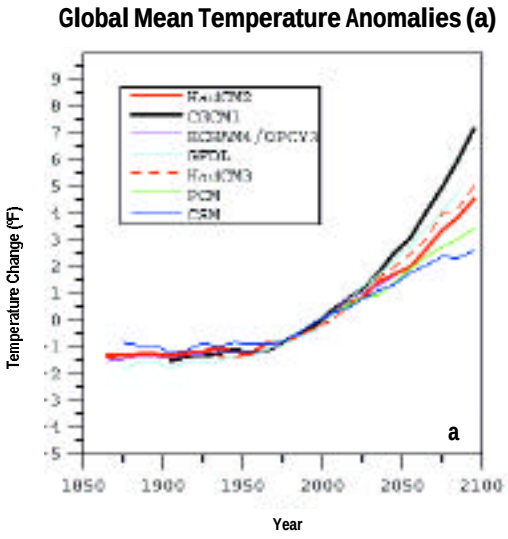

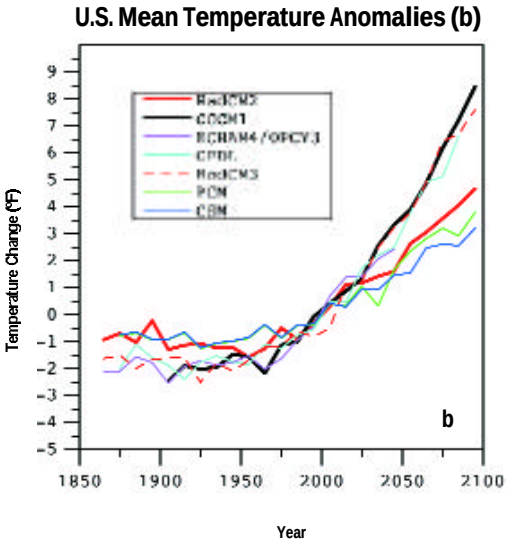

Figure 7: Comparison of the annual average changes in (a) global average surface air temperature (˚F), and (b) US average surface air temperature (˚F) from the Canadian model scenario and Hadley model scenario simulations used in the National Assessment and from the simulations of other modeling groups, including a very recent result from the Hadley Centre model version 3, Germany's Max Planck Institute/German Climate Computing Center (DKRZ), NOAA's Geophysical Fluid Dynamics Laboratory, and from the Parallel Climate and the Climate System models from the National Center for Atmospheric Research (which used a slightly lower greenhouse gas emission scenario and a significantly lower sulfate emissions scenario than the other models). Decadal means have been plotted to suppress the natural year-to-year variability. The baseline period is 1961-1990. The anomalies are with respect to the year 2000, calculating the values from a 2nd order polynomial fit over adjacent decades.

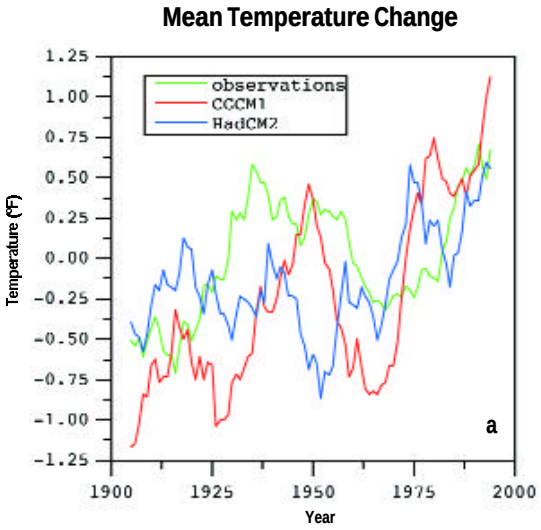

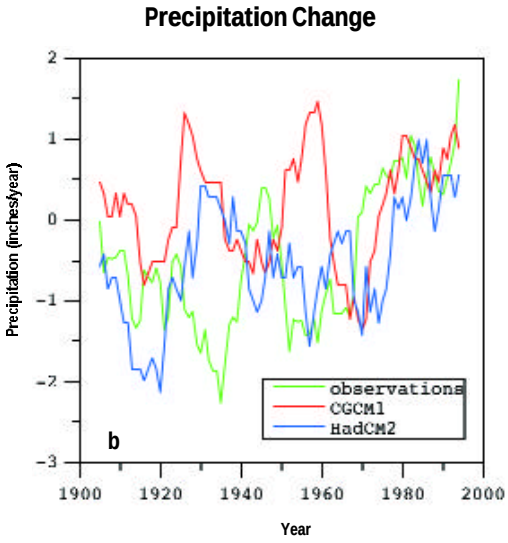

Figure 11: Time histories of the changes in (a) annual average temperature (˚F), and (b) annual total precipitation (inches per year) for the 20th century based on observations and on simulations from the Canadian and Hadley models, calculated as 10-year running means from 1900 to 2000. Mean temperature is the actual mean temperature from the models, rather than the mean of the minimum and maximum temperatures. Anomalies are shown with respect to 1961-1990. In these simulations, unlike in intercomparisons of the atmospheric models as in the AMIP project (Gates et al., 1999), the ocean temperatures are freely calculated and the concentrations of greenhouse gases and aerosols are imposed; natural forcings, such as changes in solar radiation and volcanic eruptions that are likely affecting the observed climate are not, however, being treated in the models because observations of their precise radiative influences are not available.

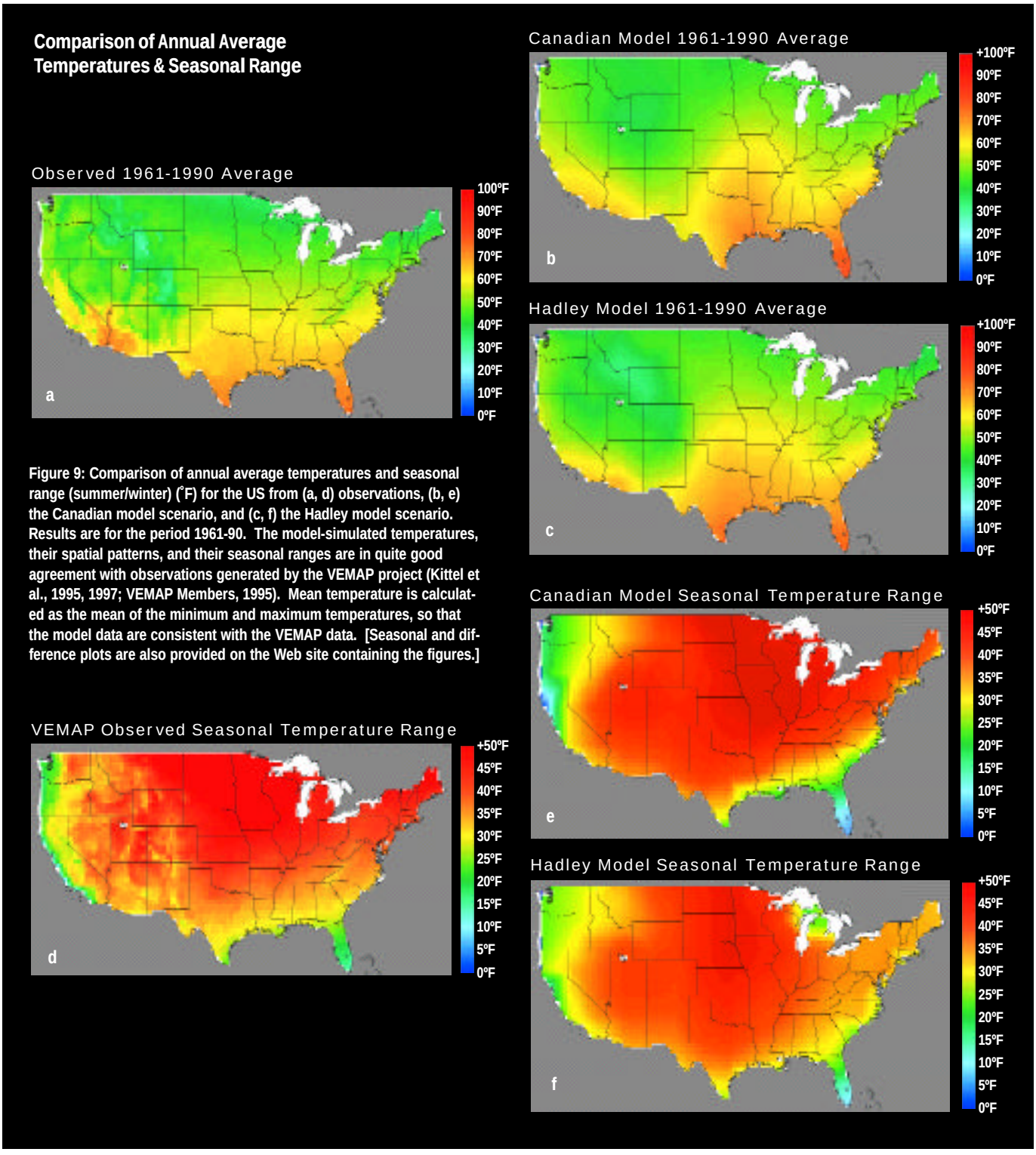

Figure 9: Comparison of annual average temperatures and seasonal range (summer/winter) (°F) for the US from (a, d) observations, (b, e) the Canadian model scenario, and (c, f) the Hadley model scenario. Results are for the period 1961-90. The model-simulated temperatures, their spatial patterns, and their seasonal ranges are in quite good agreement with observations generated by the VEMAP project (Kittel et al., 1995, 1997; VEMAP Members, 1995). Mean temperature is calculated as the mean of the minimum and maximum temperatures, so that the model data are consistent with the VEMAP data. [Seasonal and difference plots are also provided on the Web site containing the figures.]

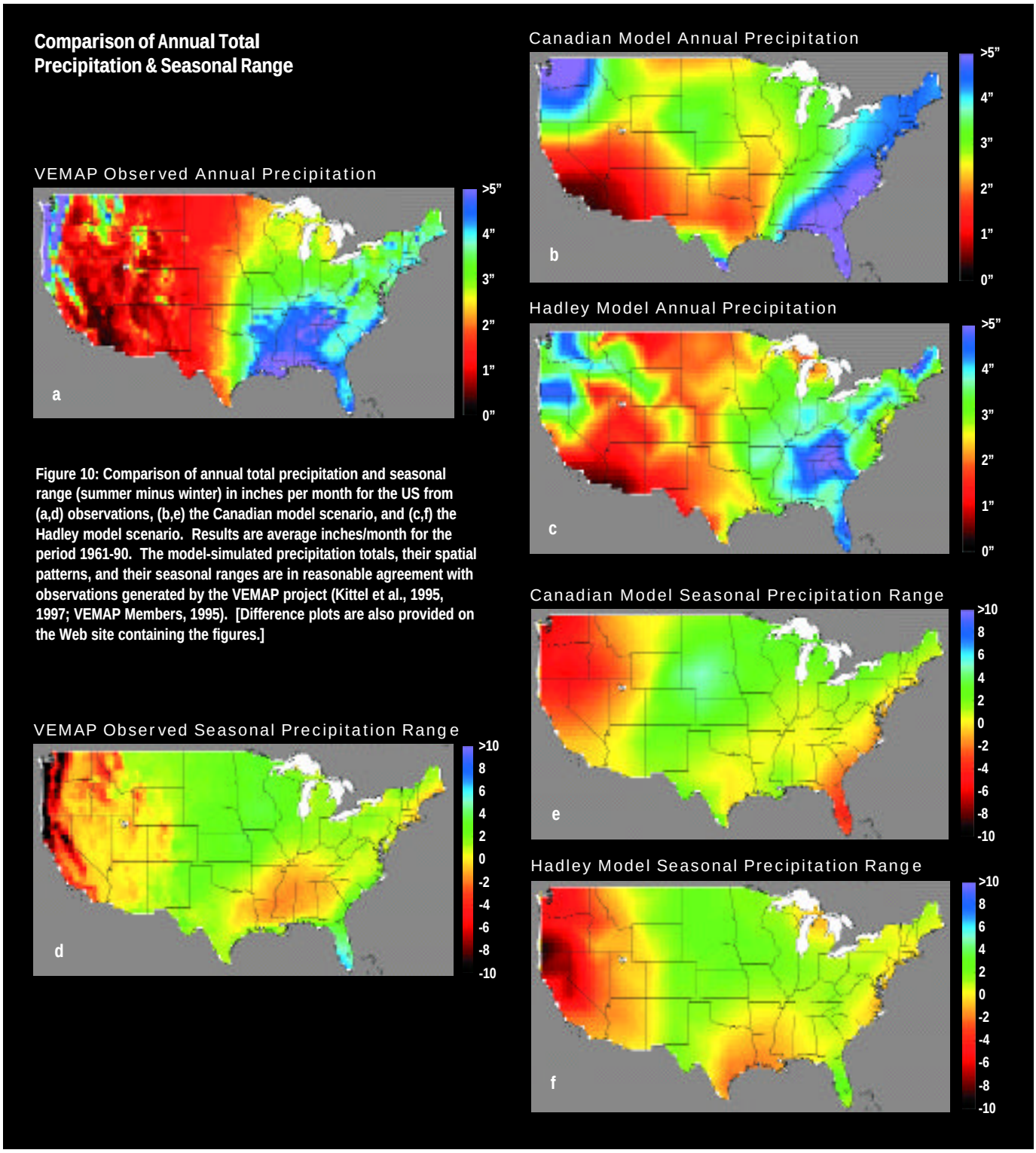

Figure 10: Comparison of annual total precipitation and seasonal range (summer minus winter) in inches per month for the US from (a,d) observations, (b,e) the Canadian model scenario, and (c,f) the Hadley model scenario. Results are average inches/month for the period 1961-90. The model-simulated precipitation totals, their spatial patterns, and their seasonal ranges are in reasonable agreement with observations generated by the VEMAP project (Kittel et al., 1995, 1997; VEMAP Members, 1995). [Difference plots are also provided on the Web site containing the figures.]

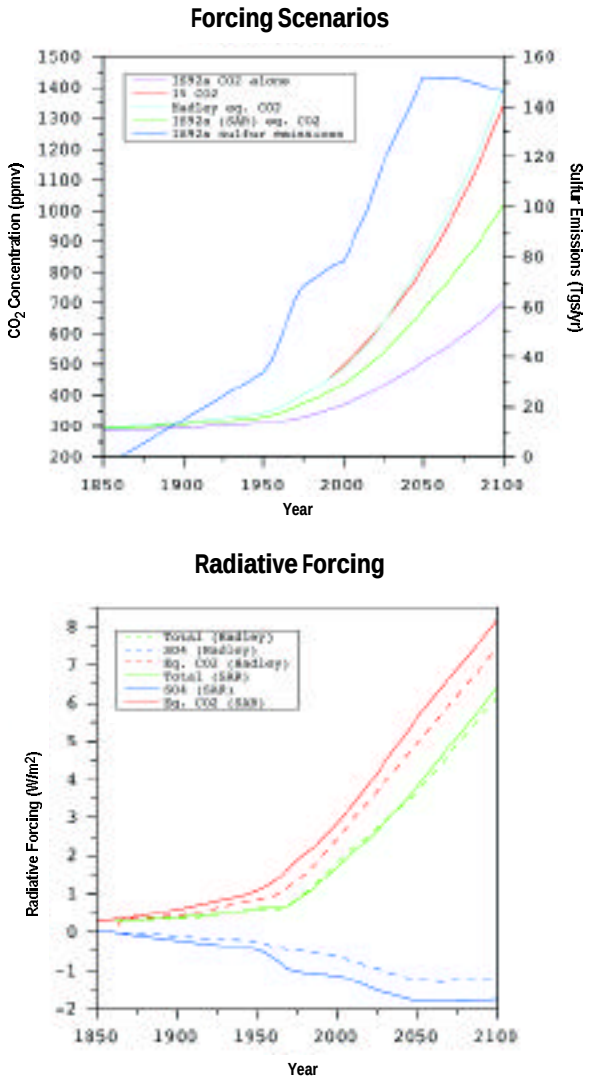

Figure 12: Comparison of different projections for aerosol effects and for (a) the CO_2 and equivalent CO_2 concentrations, and (b) the associated radiative forcings for the period 1850-2100. In the top figure, the lavender line shows the IPCC's IS92a scenario estimate of the CO_2 concentration; values prior to 1990 are based on observations. Based on this projection, the CO_2 concentration would rise to about 705 ppmv in 2100 from a level of about 353 ppmv in 1990. Because many of the climate models treat the effects of the set of human-affected greenhouse gases by use of an equivalent CO_2 concentration, the green line shows the scenario for the equivalent CO_2 concentration, which rises to about 1022 ppmv in 2100 from a value of about 410 ppmv in 1990. For this curve, the equivalent CO_2 concentration is calculated so as to incorporate the radiative effects of changes in the concentrations of all greenhouse gases using the IPCC radiative forcing equivalents (the conversion factor is 6.3 based on Appendix 2 in IPCC, 1997). The light blue line shows the equivalent CO_2 concentration that results from using the Hadley radiative forcing equivalents to approximate the IS92a scenario; the conversion factor used is 5.05 (John Mitchell, personal communication). Using the Hadley conversion factor, the equivalent CO_2 concentration for the IS92a scenario would rise to about 1409 ppmv in 2100. The red line shows that the Hadley IS92a equivalent CO_2 scenario is quite well fitted by use of a 1% per year compounded increase in the Hadley equivalent CO_2 concentration. In this case, the CO_2 equivalent concentration in 2100 reaches about 1346 ppmv. The deep blue line shows the IPCC IS92a scenario for sulfur emissions, which shows a rise until about 2050, when emissions roughly level off. While there are some differences in the projected concentrations of equivalent CO_2 between the IPCC (1996a) and the Hadley model scenario, the bottom figure shows that these differences are mostly overcome when comparing the radiative forcings that are projected by the IPCC and are actually used in the Hadley model scenario. The red and blue lines, respectively show the radiative forcings as projected by the IPCC (solid lines) and as included in the Hadley model (dotted lines). For both forcings, the Hadley model projects slightly less influence than the projections using the IPCC conversion factors. When these forcings are combined, as shown by the green lines, the net radiative forcings projected by the IPCC and used in the Hadley model 1% per year scenario are very close.

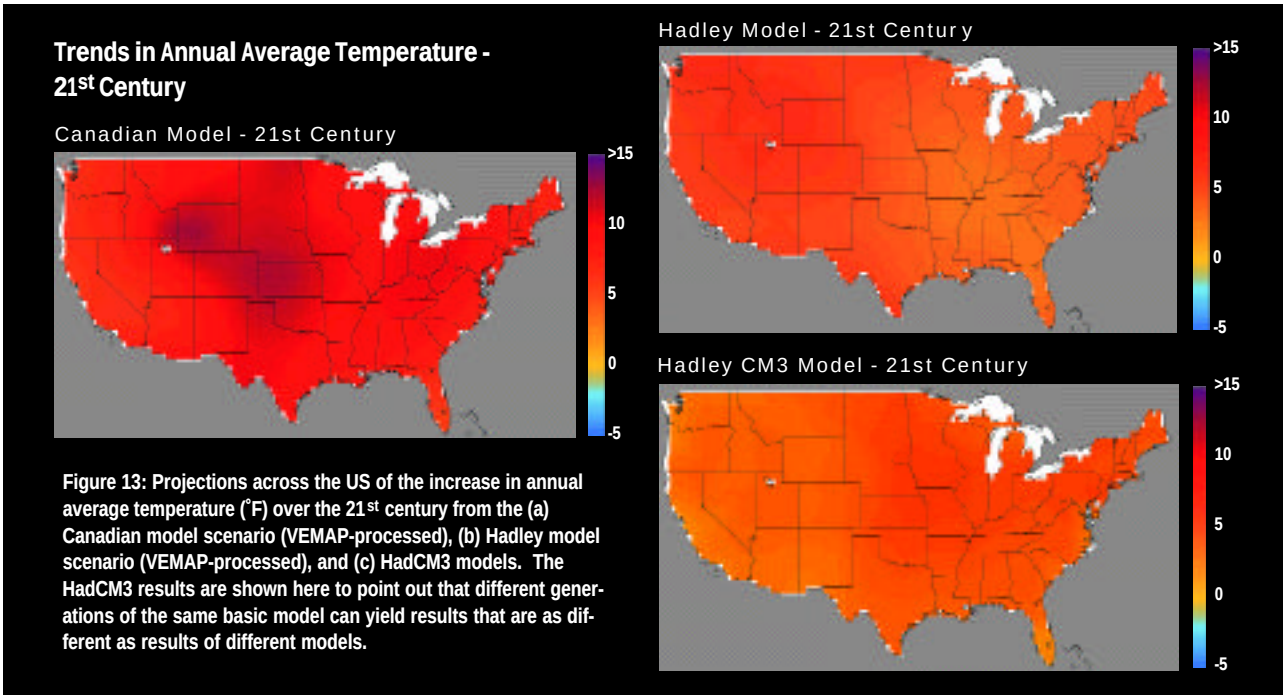

Figure 13: Projections across the US of the increase in annual average temperature (°F) over the 21st century from the (a) Canadian model scenario (VEMAP-processed), (b) Hadley model scenario (VEMAP-processed), and (c) HadCM3 models. The HadCM3 results are shown here to point out that different generations of the same basic model can yield results that are as different as results of different models.

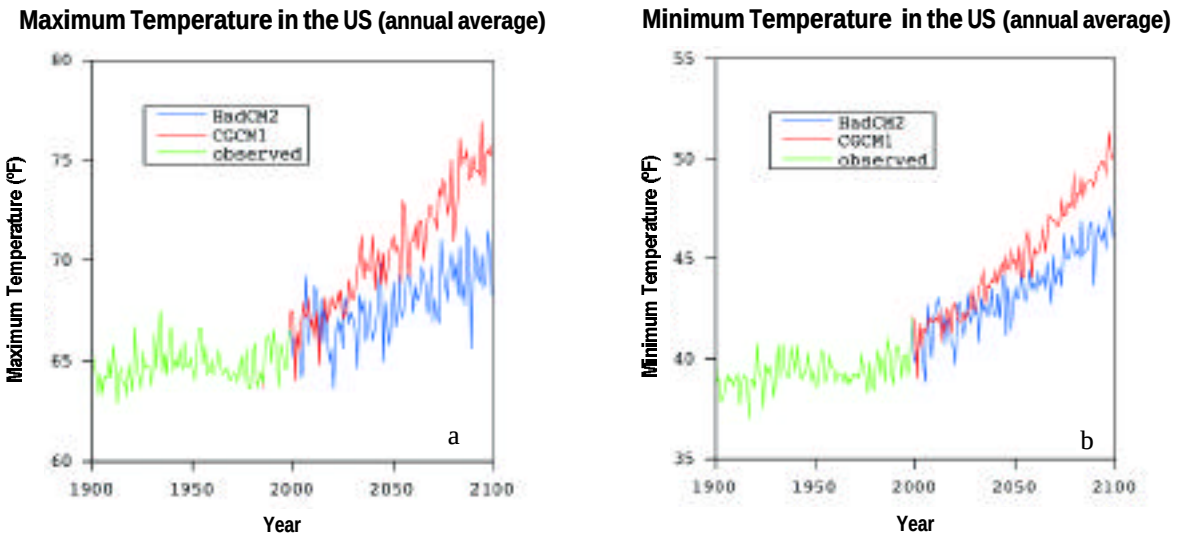

Figure 14: Time histories of (a) maximum and (b) minimum temperature over the US (˚F). The values prior to the present are based on observations from 1900-1998 (the HCN data set) and values for the future are based on the VEMAP version of the Canadian and Hadley model scenarios (i.e., in the VEMAP data sets, model projections of climate change are added to the observed 1961-90 baseline climate).

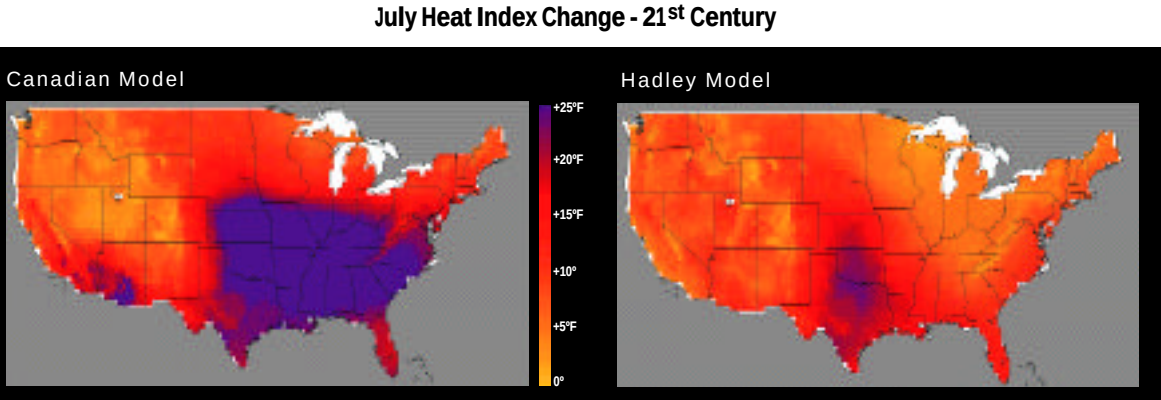

Figure 15: Projections across the US of the increase in the July heat index (˚F) over the 21st century (˚F per century) from VEMAP versions of the (a) Canadian model scenario and (b) Hadley model scenario.

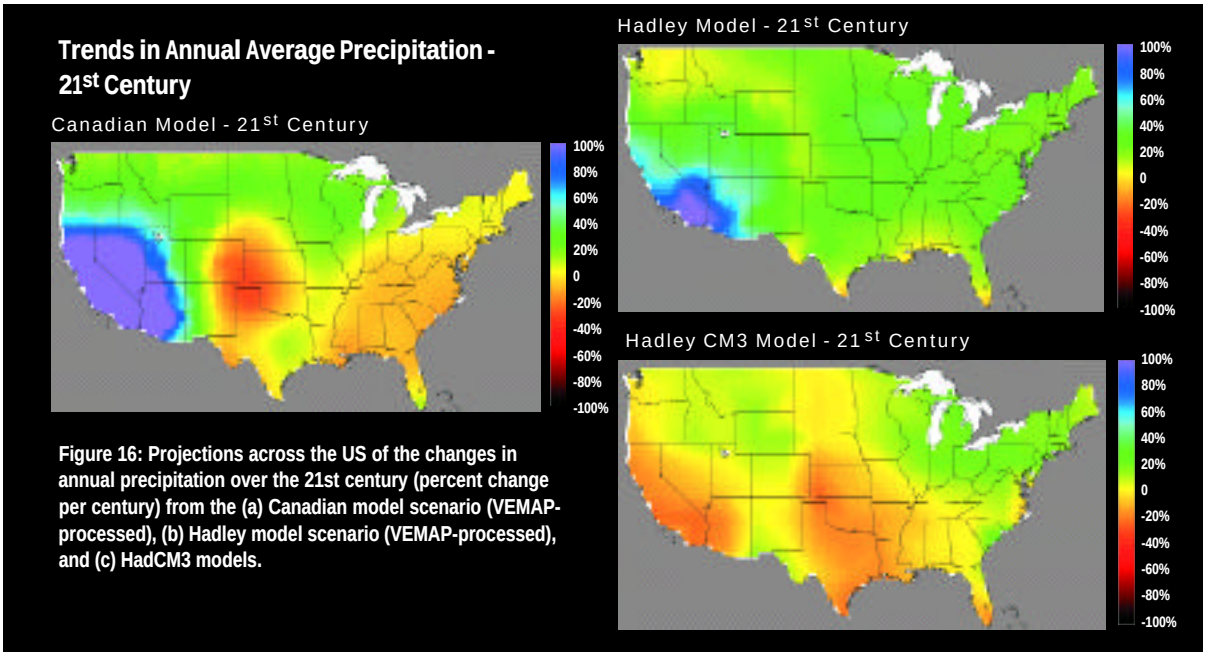

Figure 16: Projections across the US of the changes in annual precipitation over the 21st century (percent change per century) from the (a) Canadian model scenario (VEMAP-processed), (b) Hadley model scenario (VEMAP-processed), and (c) HadCM3 models.

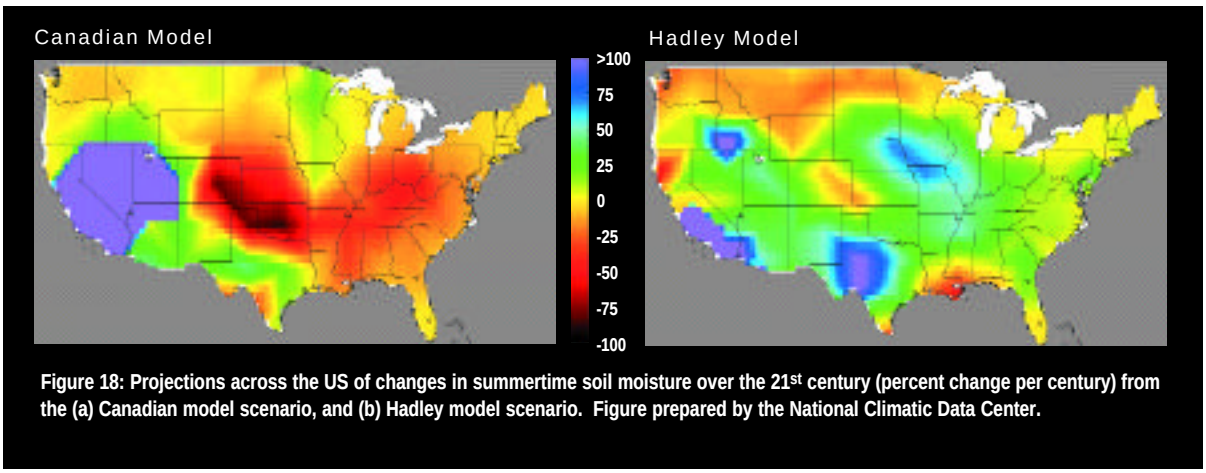

Figure 18: Projections across the US of changes in summertime soil moisture over the 21st century (percent change per century) from the (a) Canadian model scenario, and (b) Hadley model scenario. Figure prepared by the National Climatic Data Center.

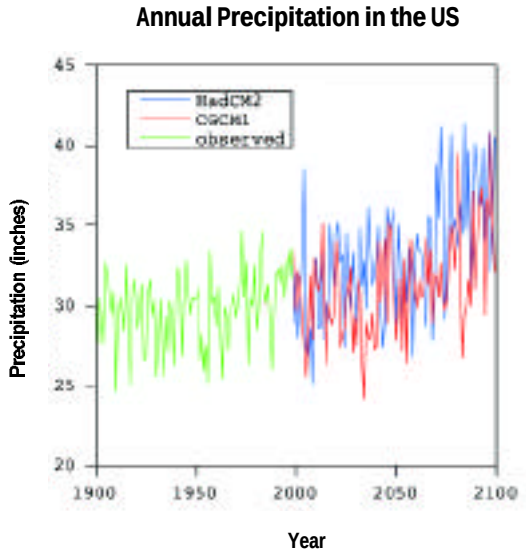

Figure 17: Time history of model projected changes in precipitation over the US (inches per year). The values prior to the present are based on observations from 1900-1998 (the HCN data set) and values for the future are based on the VEMAP version of the Canadian and Hadley model scenarios.

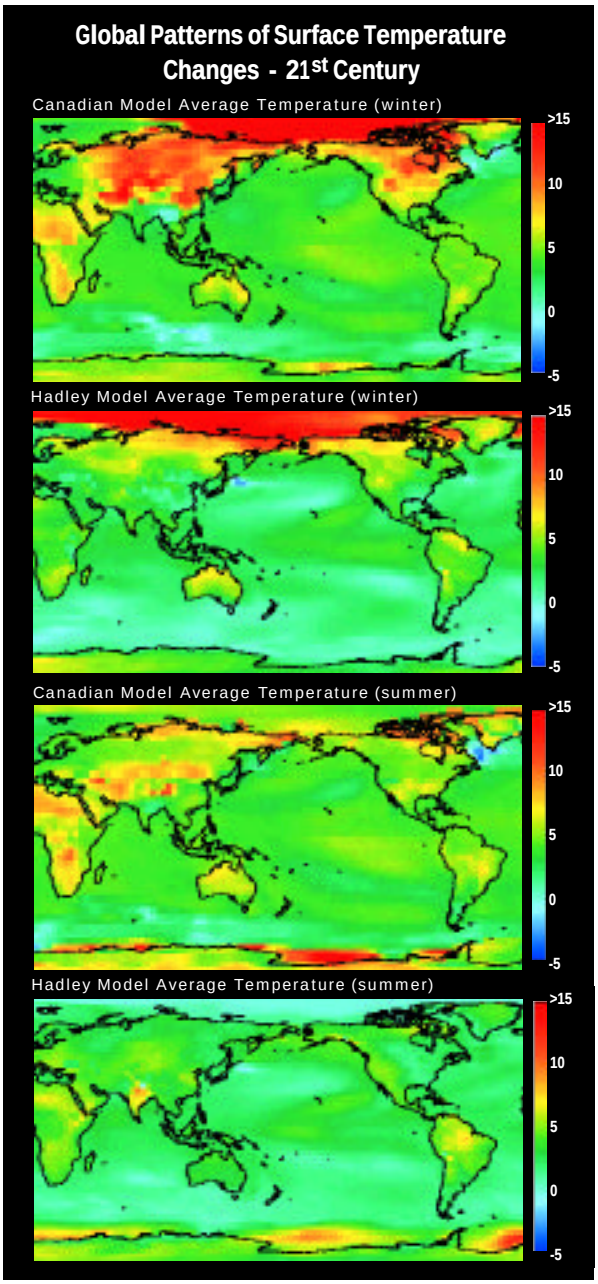

Figure 20: Global patterns of projected changes in surface temperature (˚F) over the 21st century [future (2090-2099) and modern (1961-1990)] for (a) December, January, February (DJF) from the Canadian model scenario, (b) DJF from the Hadley model scenario, (c) June, July, August (JJA) from the Canadian model scenario, and (d) JJA from the Hadley model scenario.

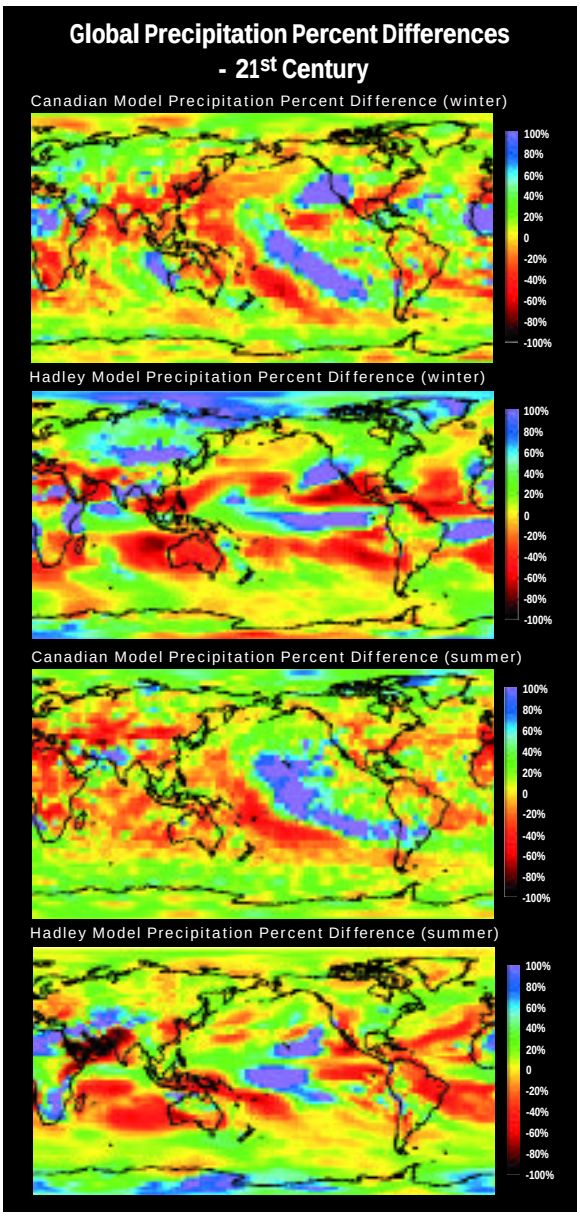

Figure 21: Global precipitation percent differences [(future - modern)/modern) x 100] for (a) December, January, February (DJF) from the Canadian model scenario, (b) DJF from the Hadley model scenario, (c) June, July, August (JJA) from the Canadian model scenario, and (d) JJA from the Hadley model scenario.

Wintertime Changes in Jet Stream and Atmospheric Circulation

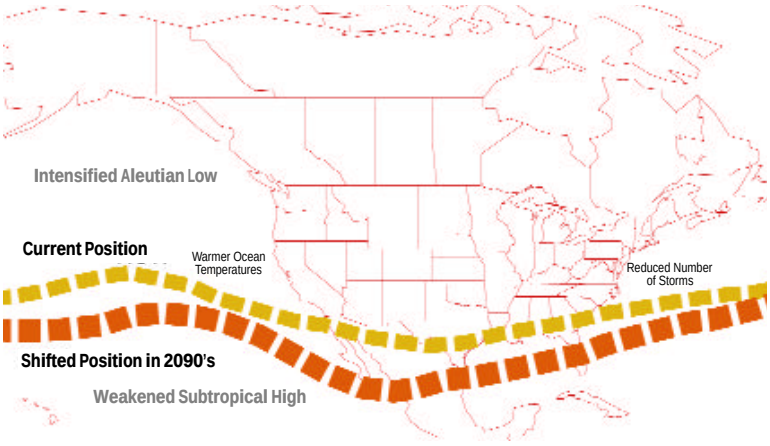

Figure 22: Schematic illustrating wintertime changes in the jet stream, pressure systems, sea surface temperatures, and storm tracks over and adjacent to North America. The Canadian and Hadley model scenarios both show: a southward-shifted jet stream over the eastern Pacific and Southwest; a southward-shifted and intensified Aleutian Low and weakened subtropical High in the West; and warmer ocean surface temperatures off the coast of California. The Canadian model scenario also shows a reduction in the number of storms along the East Coast storm track; however, the Hadley model scenario does not show this reduction nor did it develop this observed storm center in its control simulation. For more details, see Sousounis (1999).

Sea Level Rise

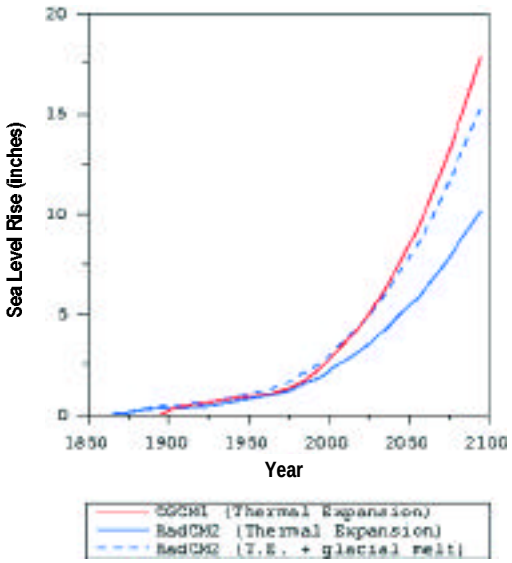

Figure 19: Historic and projected changes in sea level (inches above baseline) based on the Canadian and Hadley model scenarios. The Canadian model projection includes only the effects of thermal expansion of warming ocean waters (F. Zwiers, personal communication). The Hadley model simulation adds on the sea level increment of melting of mountain glaciers (Gregory and Oerlemans, 1998). Neither model includes consideration of possible changes of sea level (upward or downward) due to melting or accumulation of snow on Greenland and Antarctica.

Projected Changes in Intensity of National Daily Precipitation

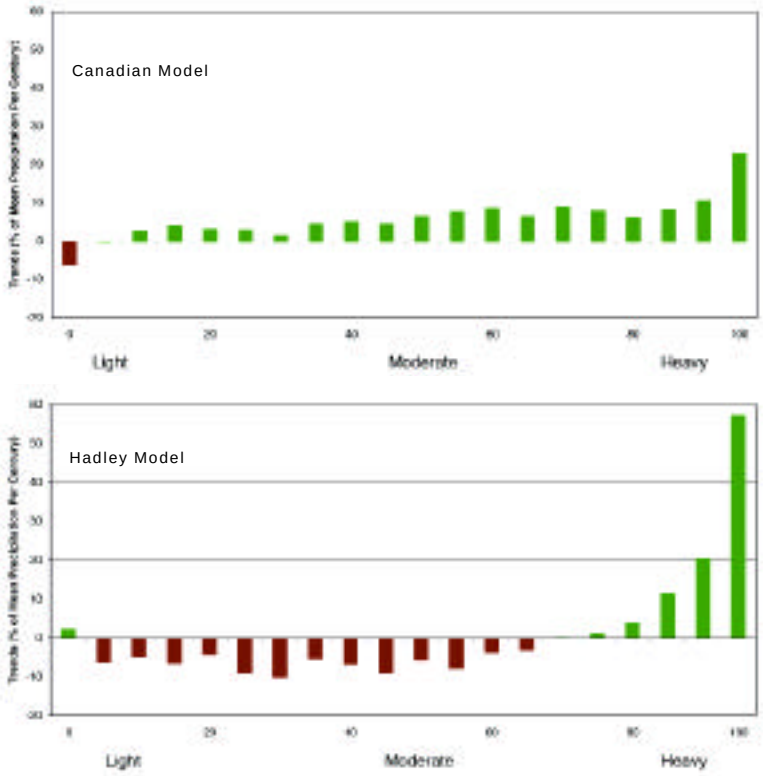

Figure 25: Bar chart showing projected changes in frequency of various types of precipitation. Both the (a) Canadian and (b) Hadley model scenarios project increases in the frequency of heavy precipitation events, intensifying the trend observed for the 20th century. Figure prepared by Byron Gleason of the National Climatic Data Center based on the methods described in Karl and Knight (1998).

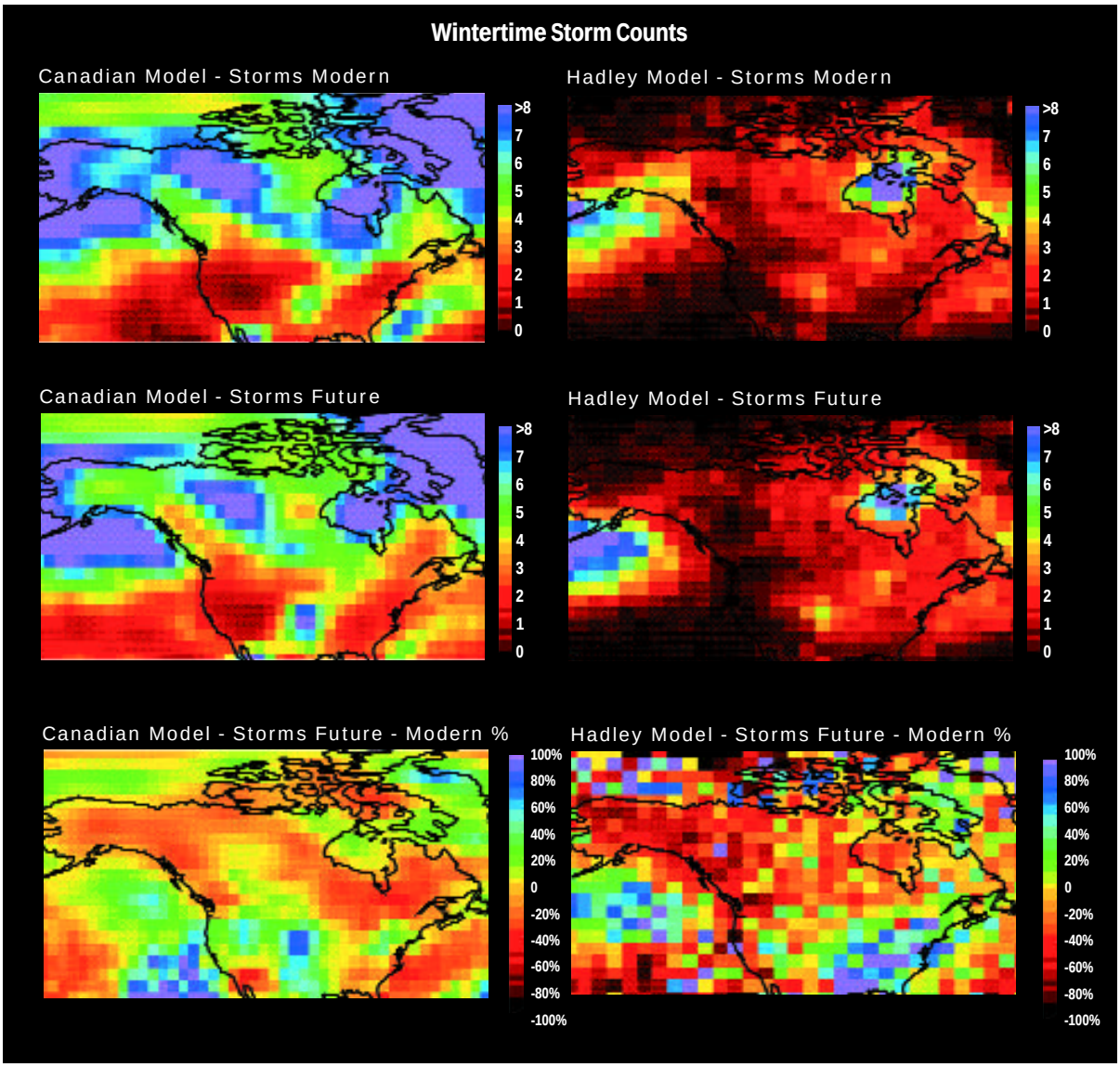

Figure 23: Wintertime (DJF) storm counts (Carnell and Senior, 1998; Lambert, 1995) from the (a) Canadian model scenario (1901-1910 total); (b) Hadley model scenario (1990-2110 mean from unforced control run); (c) Canadian model scenario (2091-2100 total); (d) Hadley model scenario (2070-2100 mean from transient run); (e) Canadian model scenario delta (c-a); and (f) Hadley model scenario delta (d-b). Units are number of winter storms per 145,000 km².

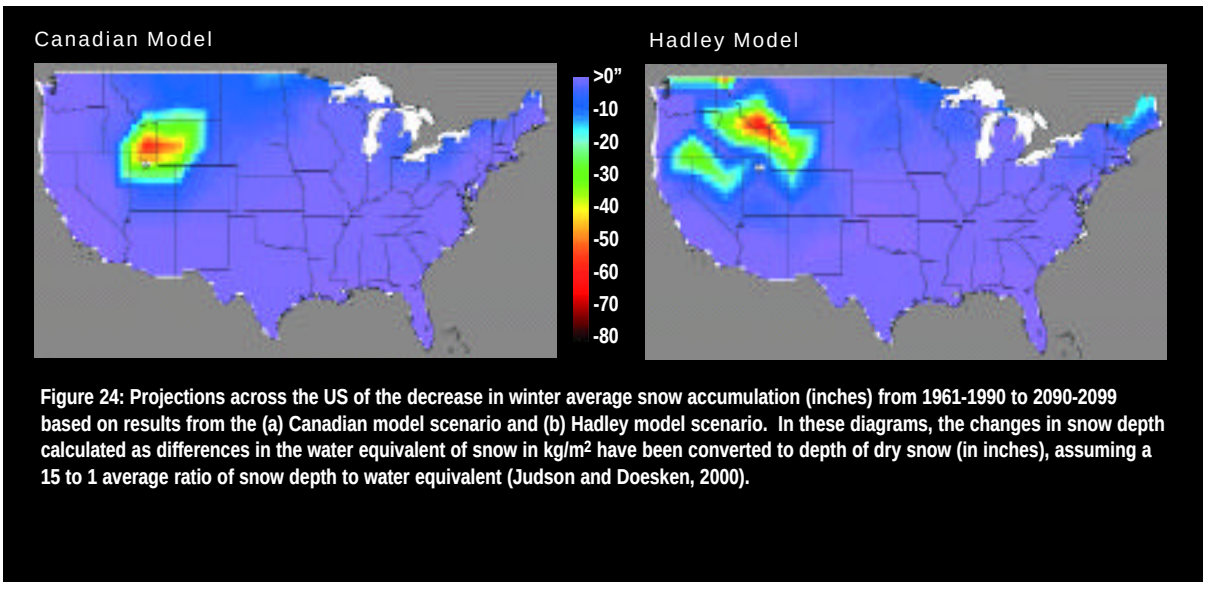

Figure 24: Projections across the US of the decrease in winter average snow accumulation (inches) from 1961-1990 to 2090-2099 based on results from the (a) Canadian model scenario and (b) Hadley model scenario. In these diagrams, the changes in snow depth calculated as differences in the water equivalent of snow in kg/m² have been converted to depth of dry snow (in inches), assuming a 15 to 1 average ratio of snow depth to water equivalent (Judson and Doesken, 2000).

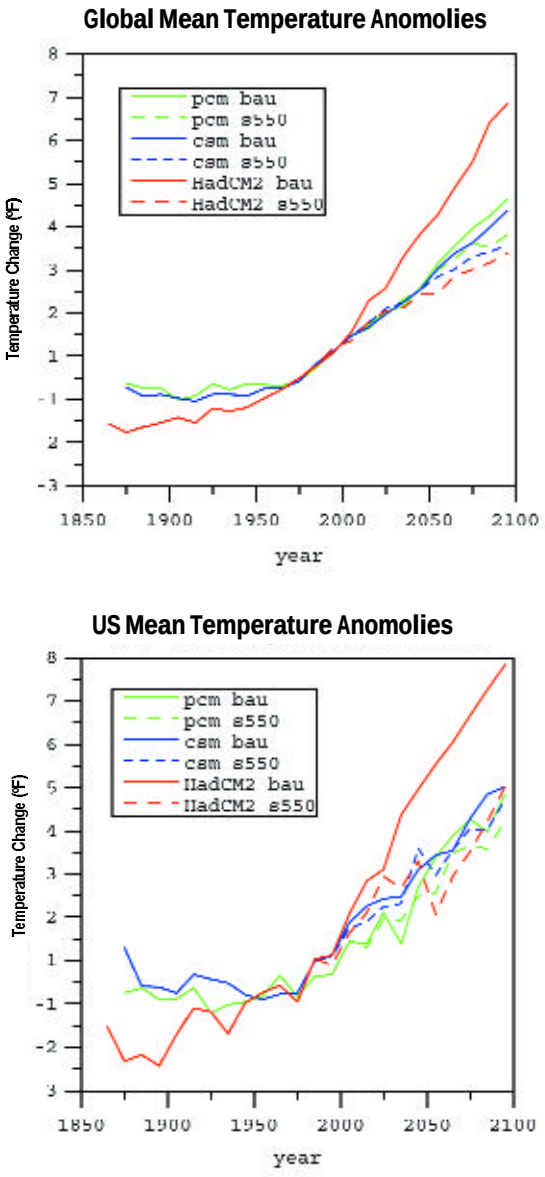

Figure 26: Comparison of the time history of the increase in annual-average surface temperature for (a) the globe and (b) the US as projected by two related models developed at the National Center for Atmospheric Research for an emission scenario where the greenhouse gas concentrations are allowed to rise without restriction (baseline) and for a case (stabilization) where steps are taken to limit the rise in the CO_2 concentration to 550 ppmv (Dai et al., 1999; Washington et al., 2000). Results are also shown for a recent Hadley model simulation (Mitchell et al., 2000). See Color Plate Appendix.

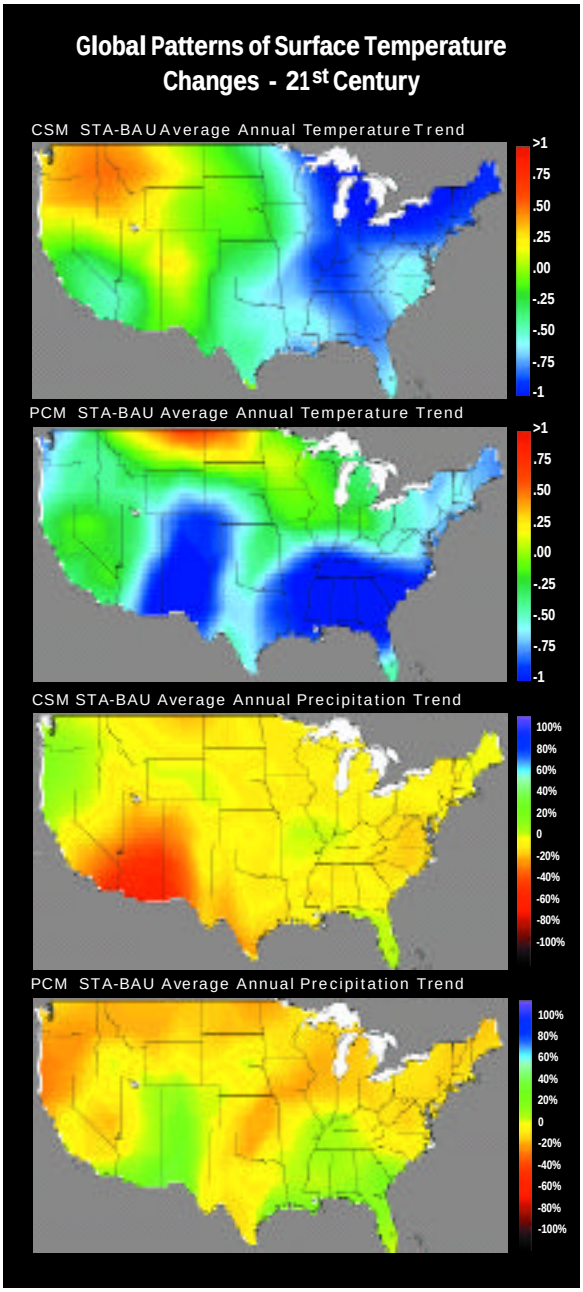

Figure 27: Patterns across the US of projected changes in the trends of annual mean surface temperature and precipitation for the 21st century assuming an emissions profile that moves toward stabilization of the CO_2 concentration at 550 ppmv in the 22nd century (STA) as compared to the baseline case (roughly case IS92a, or BAU, except projections in sulfur emissions are reduced in the CSM scenario). The projected differences in the changes that would generally be projected (case STA minus BAU) are based on results from: (a) NCAR CSM for annual mean temperature; (b) PCM for annual mean temperature: (c) NCAR CSM annual average monthly precipitation; and (d) PCM annual average monthly precipitation. Temperature trend differences are given as ˚F per 100 years. Precipitation trend differences are given in percent, with both trends calculated using a 1980-1999 baseline. Trends are derived based on a linear regression through each grid point. Results are described in Dai et al. (1999) and Washington et al. (2000). See Color Plate Appendix.